Available online at www.sciencedirect.com
SCIENCE DIRECT®
Journal of volcanology and geothermal research
ELSEVIER
Journal of Volcanology and Geothermal Research 150 (2006) 35–54
www.elsevier.com/locate/jvolgeores

Geodetic observations and modeling of magmatic inflation at the Three Sisters volcanic center, central Oregon Cascade Range, USA ☆

Daniel Dzurisin [a,*], Michael Lisowski [a], Charles W. Wicks [b], Michael P. Poland [a], Elliot T. Endo [a]

[a] *U. S. Geological Survey, David A. Johnston Cascades Volcano Observatory, 1300 S.E. Cardinal Court, Building 10, Suite 100, Vancouver, WA 98683-9589, USA*
[b] *U.S. Geological Survey, 345 Middlefield Road, MS 977, Menlo Park, CA 94025, USA*

Received 2 June 2004; received in revised form 8 December 2004
Available online 21 September 2005

Abstract

Tumescence at the Three Sisters volcanic center began sometime between summer 1996 and summer 1998 and was discovered in April 2001 using interferometric synthetic aperture radar (InSAR). Swelling is centered about 5 km west of the summit of South Sister, a composite basaltic-andesite to rhyolite volcano that last erupted between 2200 and 2000 yr ago, and it affects an area ~20 km in diameter within the Three Sisters Wilderness. Yearly InSAR observations show that the average maximum displacement rate was 3–5 cm/yr through summer 2001, and the velocity of a continuous GPS station within the deforming area was essentially constant from June 2001 to June 2004. The background level of seismic activity has been low, suggesting that temperatures in the source region are high enough or the strain rate has been low enough to favor plastic deformation over brittle failure. A swarm of about 300 small earthquakes ($M_{max}=1.9$) in the northeast quadrant of the deforming area on March 23–26, 2004, was the first notable seismicity in the area for at least two decades. The U.S. Geological Survey (USGS) established tilt-leveling and EDM networks at South Sister in 1985–1986, resurveyed them in 2001, the latter with GPS, and extended them to cover more of the deforming area. The 2001 tilt-leveling results are consistent with the inference drawn from InSAR that the current deformation episode did not start before 1996, i.e., the amount of deformation during 1995–2001 from InSAR fully accounts for the net tilt at South Sister during 1985–2001 from tilt-leveling. Subsequent InSAR, GPS, and leveling observations constrain the source location, geometry, and inflation rate as a function of time. A best-fit source model derived from simultaneous inversion of all three datasets is a dipping sill located 6.5 ± 2.5 km below the surface with a volume increase of $5.0 \times 10^6 \pm 1.5 \times 10^6$ m^3/yr (95% confidence limits). The most likely cause of tumescence is a pulse of basaltic magma intruding the upper crust along the brittle–ductile interface — a process that must occur episodically beneath the Cascade Range but in the past would have escaped detection in the absence of unusual

☆ Submitted to Journal of Volcanology and Geothermal Research (Volcano Geodesy special issue).

* Corresponding author. Tel.: +1 360 993 8909; fax: +1 360 993 8980.
E-mail address: dzurisin@usgs.gov (D. Dzurisin).

0377-0273/$ - see front matter © 2005 Published by Elsevier B.V.
doi:10.1016/j.jvolgeores.2005.07.011

seismicity. We speculate that such intrusive episodes last from days to years and are separated by quiescent periods of decades to centuries. The likelihood that the current episode at Three Sisters will culminate in an eruption is judged to be low, but the impact of an eruption could be great. The USGS has updated its volcano hazards assessment for the Three Sisters region, notified appropriate agencies and the public, and is helping to prepare an emergency coordination and communication plan.

Keywords: Three Sisters; volcanology; geodesy; radar methods; monitoring; modeling

1. Introduction

The Cascades volcanic arc, which stretches from northern California USA northward to British Columbia, Canada where it is called the Garibaldi Volcanic Belt, has produced an average of 1–2 eruptive episodes per century during the past several thousand years, including two during the 20th century: 1914–1917 at Lassen Peak, California, and 1980–1986 at Mount St. Helens, Washington. Lengthy quiescent periods between eruptions are characterized by generally low levels of seismic and hydrothermal activity, punctuated by swarms of small earthquakes that last a few days to several months. A notable exception is the Lassen volcanic center in northern California, where vigorous hydrothermal activity is manifested by numerous high temperature fumaroles, acid-sulfate hot springs, and mudpots fed from a central vapor-dominated reservoir (Muffler et al., 1982). In recent decades, sporadic earthquake swarms have been most prevalent at Mount Rainier and Mount St. Helens in Washington; Mount Hood in northwest Oregon; and Medicine Lake Volcano, Mount Shasta, and the Lassen volcanic center in northern California.

The central Oregon Cascade Range, including the Three Sisters volcanic center, produces conspicuously few earthquakes in comparison to other parts of the arc (e.g., Berg and Baker, 1963; Weaver and Michaelson, 1985). On the other hand, the central Oregon portion of the arc is the most prolific both in terms of the number of late Cenozoic vents (Guffanti and Weaver, 1988) and the Quaternary lava production rate (Sherrod and Smith, 1990).

This paper reports the results of geodetic measurements at Three Sisters, including repeated InSAR, GPS, and leveling observations, since the discovery in April 2001 of crustal uplift centered about 5 km west of the summit of South Sister. We present a source model based on simultaneous inversion of the geodetic data and discuss an inflation mechanism that is consistent with known geologic, geochemical, geodetic, and seismic constraints. Although the eruption frequency in the Cascades is low by comparison to the Aleutian volcanic arc, for example, the relatively high and increasing population densities near several Cascade volcanoes raise the stakes for natural hazards mitigation, which relies on better understanding of inter-eruption processes such as the ongoing inflation at Three Sisters.

2. Geologic setting and eruptive history

The Three Sisters volcanic center is located in the Deschutes and Willamette National Forests, mostly within the Three Sisters Wilderness in central Oregon (Fig. 1). Three Sisters is a long-lived center of basaltic to rhyolitic volcanism that has produced five large cones of Quaternary age: North Sister, Middle Sister, South Sister, Broken Top, and Mount Bachelor. South Sister, the youngest of the five, has erupted lavas ranging from basaltic andesite to rhyolite. Most, if not all, of the volcano is of late Pleistocene age. Significant growth of Middle Sister and South Sister occurred between 30 and 10 ka, when eruptions produced several large tephra falls, pyroclastic flows, lava flows, and lava domes (Fierstein et al., 2003). That activity was followed by two closely spaced eruptive sequences between about 2.2 and 2.0 ka, during which, smaller volumes of rhyolite tephra, pyroclastic flows, lava flows, and lava domes were erupted from vents on the southeast and north flanks of South Sister.

The greater Three Sisters area is volcanically complex and presents a wide range of potential eruption sites, styles, and hazards (e.g., Taylor et al., 1987; Scott and Gardner, 1990; Scott et al., 2001). Past events ranged from fissure-fed basalt lava flows to

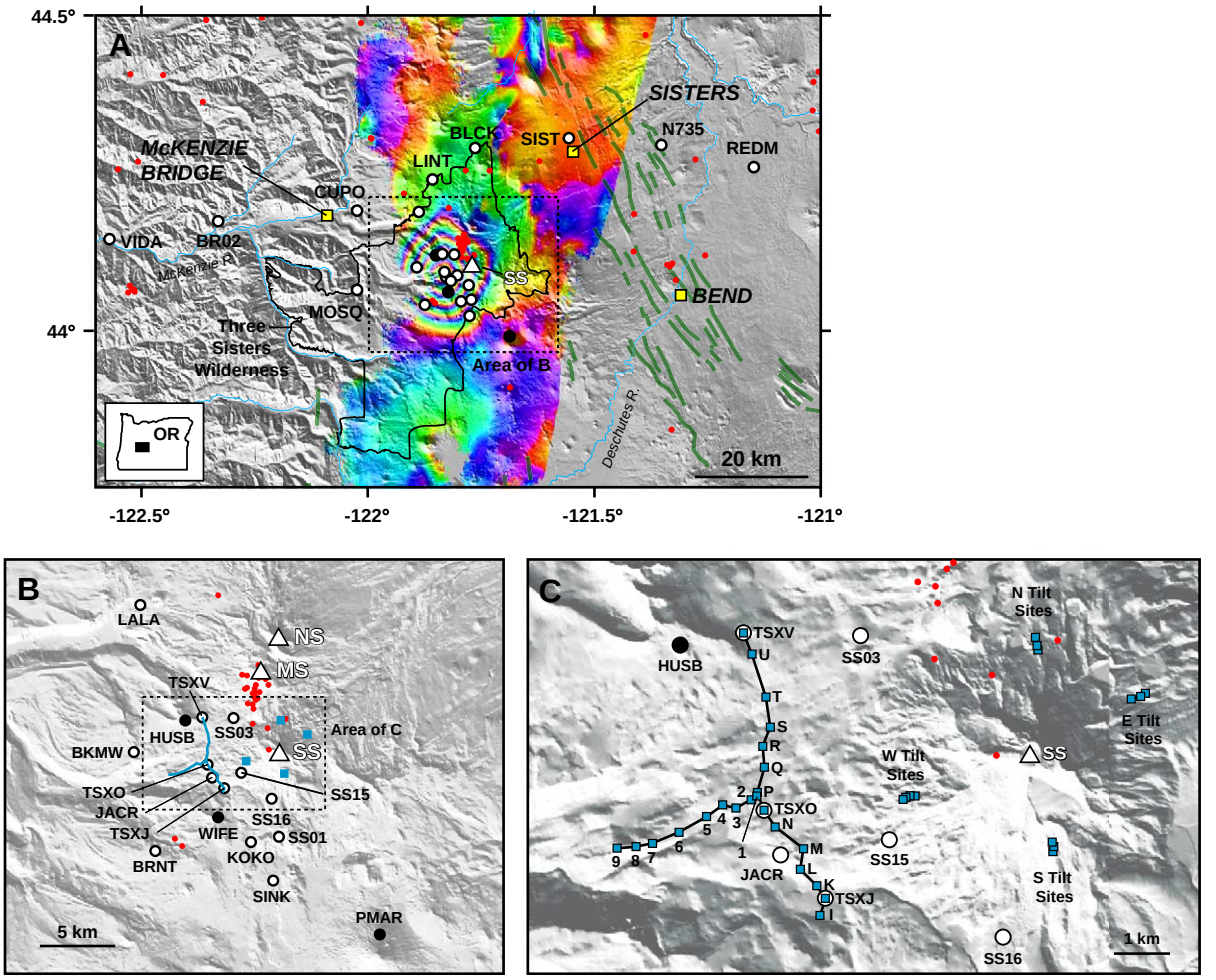

Fig. 1. Maps at progressively smaller scale centered at the Three Sisters volcanic center in central Oregon showing the locations of campaign GPS marks (white circles), continuous GPS stations (black circles), leveling transects (blue lines and squares in B, C), and historical seismicity (small red dots). Triangles mark the locations of North Sister (NS), Middle Sister (MS), and South Sister (SS). A, Shaded relief map with Quaternary faults (green lines), major drainages (thin blue lines), GPS stations, and epicenters of earthquakes recorded between 1980 and April 30, 2004. Cluster of epicenters near South Sister represents the March 2004 earthquake swarm. Earthquake data are from the Pacific Northwest Seismograph Network catalog. Interferogram for the period 1995–2001 shows ~14 cm of uplift centered ~5 km west of the summit of South Sister. Marks along the McKenzie River GPS traverse were observed by repeated campaigns in 1999. Dashed box indicates the area shown in B. B, Blue lines near the center are leveling transects surveyed in 2002 and 2003. Blue squares represent short (200–320 m long) tilt-leveling lines on the flanks of South Sister that were established in 1985 and remeasured in 1986 and 2001. Other symbols are the same as in A. Dashed box indicates the area shown in C. C, Close-up view of the deforming area west of South Sister. Blue squares in west part of figure represent marks along the leveling transects that are shown as blue lines in B; blue squares in east part of figure (short radial transects on the flanks of South Sister) represent marks along the tilt-leveling lines that are shown as blue squares in B. Some leveling marks are also used as GPS marks. James Creek Shelter is near mark TSXO. Other symbols are the same as for A and B. (For interpretation of the references to colour in this figure legend, the reader is referred to the web version of this article.)

explosive rhyolitic plinian eruptions. Tens of vents spread over a 400-km^2 area have erupted in the past 4000 yr. During Holocene time, eruptions have been more frequent immediately north of Three Sisters. As recently as 1.6 to 1.2 ka, dominantly effusive eruptions of basaltic and andesitic lavas have built large shield volcanoes such as Belknap Crater and isolated cinder cones and lava flows such as Collier Cone. In

the area that is currently deforming, excluding products from South Sister, dated units include: (1) dacite of Dew Lake (32 ± 2 ka); (2) basalt of vent knob 6482 (148 ± 4 ka); and (3) basalt of The Husband (149 ± 5 ka) (Fierstein et al., 2003).

3. Previous work

In addition to the geologic mapping and petrologic studies mentioned above, two bodies of earlier work are pertinent here. One is the discovery in April 2001 of surface tumescence west of South Sister using InSAR, and the other is the earlier detection of chloride and temperature anomalies in Separation Creek, which drains the deforming area (Fig. 1). The InSAR results constrain the source location and time history of the inflation, while the geochemical data bear on the inflation mechanism and provide a broader volcanological context for its interpretation.

3.1. InSAR observations, 1992–2000

Crustal uplift at Three Sisters was discovered by Wicks et al. (2002a), who formed several interferograms from radar images acquired by the European Space Agency's Earth Resources Satellites, ERS-1 and ERS-2, from 1992 to 2000. Deformation profiles across unwrapped versions of the interferograms reveal progressive uplift of an area about 20 km across centered about 5 km west of the summit of South Sister. Wicks et al. (2002a) concluded that most if not all of ~10 cm of uplift occurred between September 1998 and October 2000. They modeled the deformation source as an inflating point source (Mogi, 1958) at a depth of 6.5 ± 0.4 km with a volume increase of $23 \times 10^6 \pm 3 \times 10^6$ m^3, which they interpreted as inflation of a crustal magma reservoir by intrusion.

3.2. Separation Creek chloride and temperature anomalies

Reconnaissance stream sampling in the central Oregon Cascades in 1990 revealed an anomalously high chloride concentration (>0.5 mg/L) in Separation Creek, the only such anomaly identified in the Quaternary High Cascades, several years prior to the onset of uplift (Ingebritsen et al., 1994). Additional sampling through 1998 showed that perennial streams in the Separation Creek drainage are anomalous in both temperature and chloride, up to 5 °C and 20 mg/L, respectively, above normal cold springs in the region (Iverson, 1999). The discovery of uplift prompted new and expanded geochemical investigations starting in 2001. Based mainly on the geochemical evidence, Evans et al. (2004) inferred the presence of a long-lived hydrothermal system powered by magmatic heat, which is consistent with the intrusion mechanism proposed by Wicks et al. (2002a) to account surface uplift since 1998.

4. Geodetic data, 1985–2003

Geodetic datasets for the Three Sisters area include: (1) electro-optical distance meter (EDM) and tilt-leveling surveys at South Sister in 1985 and 1986; (2) campaign GPS observations at South Sister in 2001 and at newly established marks throughout the deforming area each summer from 2001 to 2003; (3) leveling surveys along trails near the center of uplift in 2002 and 2003; (4) continuous GPS (CGPS) observations from station HUSB near The Husband starting in May 2001 and from station PMAR at Mount Bachelor starting in April 2002; and (5) yearly InSAR observations from 1992 to 2001 (Fig. 1). The U.S. Geological Survey (USGS) installed a third continuous GPS station near The Wife in July 2004 and repeated campaign GPS and leveling surveys in August 2004. The campaign GPS and leveling data from 2004 are not included in this analysis; they indicate that deformation continued during 2003–2004 but the details are yet to be finalized. No useful interferograms were obtained for 2002 or 2003, but radar images of the Three Sisters area suitable for interferometry are being acquired by Envisat (European Space Agency) and Radarsat-1 (Canadian Space Agency), which will be joined in the near future by Japan's Advanced Land Observing Satellite (ALOS) and Radarsat-2.

4.1. Tilt-leveling, EDM, and campaign GPS at South Sister, 1985–2001

The USGS established tilt-leveling and EDM networks at South Sister in 1985 and repeated the sur-

veys in 1986. There were no significant differences between the 1985 and 1986 results, which constitute a baseline set of observations (Yamashita and Doukas, 1987; Iwatsubo et al., 1988).

4.1.1. Tilt-leveling, 1985–2001

The tilt-leveling network at South Sister consists of 4 radial lines, each 200–320 m long with 3 or 4 survey marks (metal disks) attached to rock. The lines are located on the south, west, north, and east flanks of South Sister at elevations of 2510, 2250, 2320, and 2310 m, respectively. Owing to their orientations and relative distances from the center of inflation, the lines on the west and east flanks, in that order, are more sensitive to the deformation source. The lines on the north and south flanks are relatively insensitive to the source because they are sub-parallel to contours of equal uplift at those sites (Fig. 1A).

We determined elevation differences between adjacent marks by differential leveling that conformed in most respects to standards for first-order, class II surveys established by the National Geodetic Survey (Federal Geodetic Control Committee, 1984). The only departure is that a few readings were made on the lower 0.5 m of the rods — a consequence of the relatively steep terrain and time constraints. Any resulting refraction error is likely to be negligible because: (1) the lines are short; (2) most of the shots

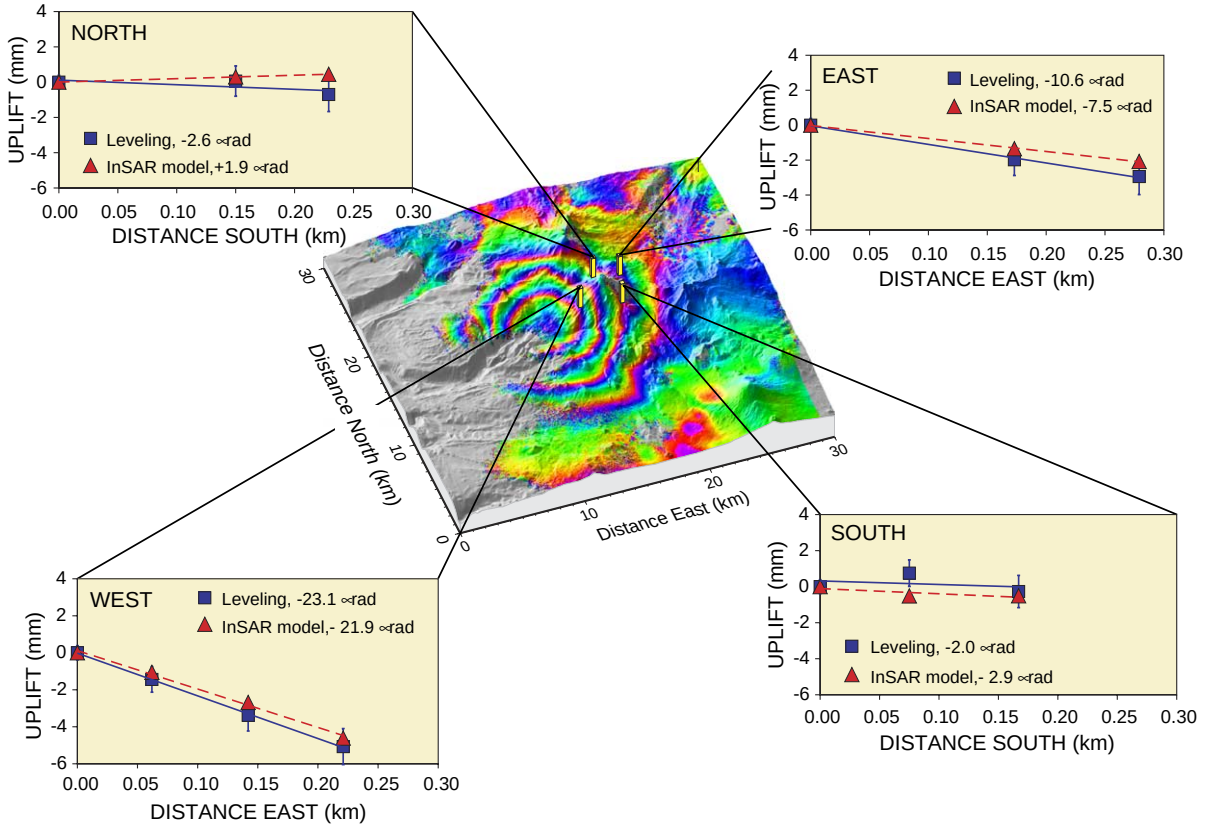

Fig. 2. Relative height changes between marks (blue squares) and average surface tilts (blue lines) at four tilt-leveling lines on South Sister for the period 1986–2001. For each line, height changes are relative to the mark farthest from the summit. Red triangles are values predicted by a best-fit point source model based on an interferogram for the period 1996–2000 (Wicks et al., 2002a). The interferogram shown here is for the period 1995–2001. The summit of South Sister is near the center of four yellow bars near the center of the figure, which represent the tilt-leveling lines. The lines are radial to the summit, so only those on the west and east flanks are sensitive to the deformation source. Each interferometric fringe (full color cycle) represents 2.83 cm of range change between the ground and the satellite. (For interpretation of the references to colour in this figure legend, the reader is referred to the web version of this article.)

were short (6–20 m); and (3) the lines are above tree line and exposed to persistent breezes that mix the atmosphere near the ground. We applied all appropriate corrections to the field observations, including those for rod scale, temperature, level collimation, and refraction. The Wild NA2 level used in 1985 and 1986 was fitted with a magnetic shield to eliminate the need for magnetic corrections, and the Leica NA3003 digital level used in 2001 is not subject to magnetic errors. Differential astronomic and orthometric corrections are negligible for lines this short (Balazs and Young, 1982).

Relative height changes (tilts) measured at the South Sister tilt-leveling stations from 1985–1986 to 2001 are shown in Fig. 2, together with the values predicted by a best-fit model based on the InSAR results for 1996–2000. General agreement between the tilts measured by leveling and those predicted from the InSAR data suggests that the uplift did not start before 1996; otherwise, the measured tilts would exceed the predicted values. Based on several interferograms that span, as a group, the period 1992–2000, Wicks et al. (2002a) concluded that uplift began in late 1997 or early 1998.

4.1.2. EDM and campaign GPS, 1985–2001

The EDM network established at South Sister in 1985–1986 consists of 16 marks at elevations that range from 2025 to 3156 m. Line-lengths and zenith angles were measured for 24 pairs of intervisible

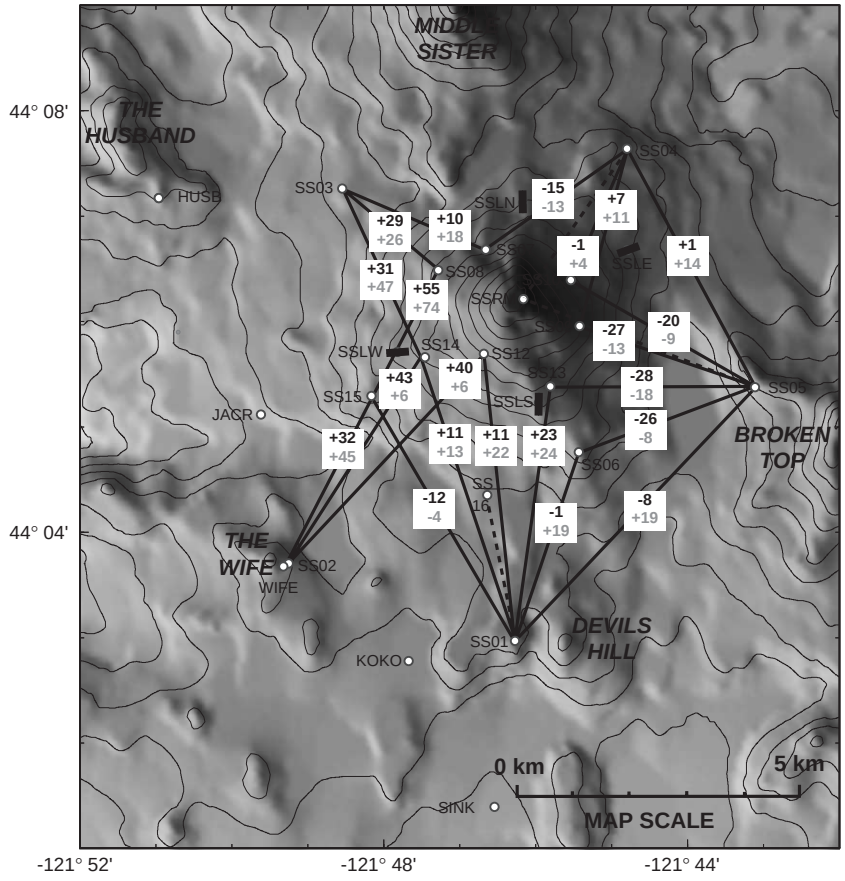

Fig. 3. Observed (black, upper) and predicted (gray, lower) line-length changes in millimeters at South Sister measured by comparison of EDM (1985, 1986) and GPS (2001) observations. Predicted values are from the best-fit point source model based on the 1996–2000 interferogram (Wicks et al., 2002a), which is shown in Fig. 2. Presumed accuracy of the EDM measurements is about ± 10 mm. Short, heavy black lines (SSLW, SSLN, SSLE, and SSLS) represent the tilt-leveling stations that are also shown in Fig. 1 A, B.

marks from 5 instrument stations near the base of the volcano to others high on the flanks. When the marks were next recovered in 2001, one near the summit had been disturbed and was unusable but the others were observed with GPS for periods of 12–24 h each. Line-length changes computed from the 1985–1986 and 2001 observations are roughly consistent with the model of Wicks et al. (2002a), with the largest changes in the western part of the network nearest the deformation center, but the results are noisy (Fig. 3).

Lisowski and Prescott (1981) reported that the repeatability for short lines (1–3 km) measured with instrumentation and procedures similar to those used in 1985 and 1986 was about 5 mm. The lines-of-sight at South Sister are steep and, even though temperature and humidity measurements were made both at the endpoints and from a helicopter flying along the lines during the EDM measurements, substantial uncorrected variations in the atmospheric index of refraction are possible. To account for meteorological uncertainty, we included quadrature scale error of 2 parts per million (ppm) in the EDM line-length measurements. This is a larger value than is typically used for this type of measurement (~1 ppm). Considering the problems introduced by steep topography, we chose to err on the side of overestimating the uncertainties, which are given (in meters) by:

$$\sigma(\Delta L) = \sqrt{\left(5 \times 10^{-3}\right)^2 + \left(2 \times 10^{-6} \cdot L\right)^2} \qquad (1)$$

For the line-lengths involved (2–6 km), the uncertainties are in the range 7–11 mm (Table 1).

To estimate the uncertainty in line-length measurements derived from GPS data, we relied on results reported by Savage et al. (1996), who found good agreement between distances measured with GPS and

Table 1
Line-length changes at South Sister from EDM (1985 and 1986) and GPS (2001) measurements

Line	(BM-BM)	Line length, L (m)			Line length change, ΔL (m)	Standard deviation, $\sigma(\Delta L)$ (m)
		1985 EDM	1986 EDM	2001 GPS		
1	SS03-SS07	2786.239	2786.236	2786.248	0.010	0.075
2	SS04-SS07	3065.245	3065.243	3065.229	−0.015	0.078
3	SS04-SSRM	3328.312	3321.254	3325.393	*	*
4	SS04-SS10	2536.564	2536.569	2536.566	−0.001	0.071
5	SS04-SS09	3263.211	3263.223	3263.218	0.007	0.081
6	SS04-SS05	4756.635	4756.626	4756.631	0.001	0.098
7	SS05-SS10	3752.340	3752.335	3752.317	−0.020	0.087
8	SS05-SSRM	4419.695	4426.028	4428.568	*	*
9	SS05-SS09	3293.252	3293.241	3293.220	−0.027	0.081
10	SS05−SS13	3608.944	3608.946	3608.917	−0.028	0.085
11	SS05-SS6	3304.364	3304.362	3304.337	−0.027	0.081
12	SS05-SS01	6151.456	6151.455	6151.448	−0.008	0.111
13	SS01-SS06	3521.068	3521.042	3521.055	−0.001	0.084
14	SS01-SS13	4556.192	4556.192	4556.215	0.023	0.096
15	SS01-SS12	5125.162	5125.174	5125.180	0.012	0.101
16	SS01-SS16	2614.367	2614.376	2614.370	−0.002	0.072
17	SS01-SS14	5256.146	5256.146	5256.157	0.011	0.103
18	SS01-SS15	4993.690	4993.686	4993.676	−0.012	0.100
19	SS02-SS12	5085.010	5085.023	5085.056	0.040	0.101
20	SS02-SS14	4372.910	4372.916	4372.956	0.043	0.094
21	SS02-SS15	3287.013	3287.015	3287.047	0.032	0.081
22	SS02-SS08	5807.041	5807.068	5807.110	0.055	0.108
23	SS03-SS14	3329.333	3329.341	3329.368	0.031	0.082
24	SS03-SS08	2260.467	2260.458	2260.491	0.029	0.067

The two sets of EDM measurements were averaged to obtain a single baseline dataset for 1985–1986. The line length changes in column 6 are the differences between the 2001 value and the average of the 1985 and 1986 values.

* Station SSRM was disturbed between the 1985 and 1986 surveys, and again between the 1986 and 2001 surveys.

EDM. Based on their analysis, we assumed uncertainty of 5 mm in our GPS-derived line lengths. The resulting uncertainty in line-length changes based on comparison of the EDM and GPS data is ~10 mm (Table 1). The observed changes, similar to the tilt-leveling results, are consistent with the inference from InSAR that little or no deformation occurred prior to 1998 (i.e., the observed line-length changes for 1985–1986 to 2001 are comparable to those predicted by a model based on InSAR observations for 1998 to 2001).

Owing to the relatively small signal-to-noise ratio, we did not include the EDM/GPS data for 1985–2001 in our source-model inversions. Likewise, we excluded the 1985–2001 tilt-leveling measurements at South Sister because so few data points would not appreciably affect the modeling results. As mentioned above, the primary value of the 1985–1986 data is in helping to constrain the onset of deformation through comparison with the more recent InSAR results.

4.2. Campaign GPS, 1999–2003

The USGS established the McKenzie River campaign-GPS traverse in 1999 to measure deformation across the central Oregon Cascades near Three Sisters (Fig. 1). We included data from a subset of that network in our analysis. In September 2001, we resurveyed the 16-station South Sister EDM network (Iwatsubo et al., 1988) with GPS and added 18 new marks, 13 of which are within 10 km of the deformation center. We added 12 more marks within 7 km of the deformation center in 2002 and in 2003 we tied several difficult-to-access marks to new marks nearby that are easier to access (Fig. 1). All of the marks are attached to bedrock or large buried boulders. Helicopter support was available for the 2001 survey, but the 2002 and 2003 surveys were accomplished on foot. For that reason, we observed all of the 1985–1986 marks on South Sister in 2001, but only a few of them in 2002 and 2003. For each of the surveys, we observed marks continuously for at least 8 h on several days using Trimble 4700, Ashtech Z-12, or Trimble 4000 SSi receivers with geodetic antennas.

We processed the GPS data with the GIPSY/OASIS II software using the point-positioning method (Zumberge et al., 1997), following the procedures outlined by Savage et al. (2001b). We computed positioning solutions in the ITRF97 reference frame and transformed them into a nominally stable North American Plate reference frame. We then adjusted the daily solutions, which include about 50 global stations with well-determined velocities, using QOCA (Dong et al., 1998). QOCA applies a Helmet transformation to the loosely constrained daily solutions to produce solutions in which the velocities of the global reference stations are most consistent with their known values. No constraints are applied to the velocities of stations in the local network. The computed local station velocities (Fig. 4) show a pattern of radial deformation in the uplifting area and north-northeast motion of the network as a whole. Previous studies (Svarc et al., 2002; McCaffrey et al., 2000) showed that the region is undergoing a rigid-body rotation about a pole located in eastern Oregon. To determine the pattern and rate of volcanic deformation, we first had to remove this tectonic motion.

Using the pole and rotation rate derived by Svarc et al. (2002), we found that a small amount of residual rotational motion remained in our velocity field. We then applied the method of Savage et al. (2001a,b) to compute a best-fitting pole, uniform rotation rate, and residual strain, excluding stations within the uplifting area. The small number of stations and short time interval spanned by the measurements resulted in poorly determined results. We then repeated the QOCA adjustment for velocities and rotation/strain determination, this time including regional campaign and continuous GPS stations. The calculated pole, rotation rate, and residual strain accumulation from this and previous analyses are summarized in Table 2. The observed and corrected velocities in the Three Sisters area are summarized in Table 3 and shown in Fig. 4.

4.3. Leveling, 2002–2003

When the comparison of 1985–1986 and 2001 tilt-leveling results from South Sister turned out to be consistent with the source area and inflation history determined from InSAR, we installed new leveling lines closer to the source that are more easily accessible by hiking. In September 2002, we established

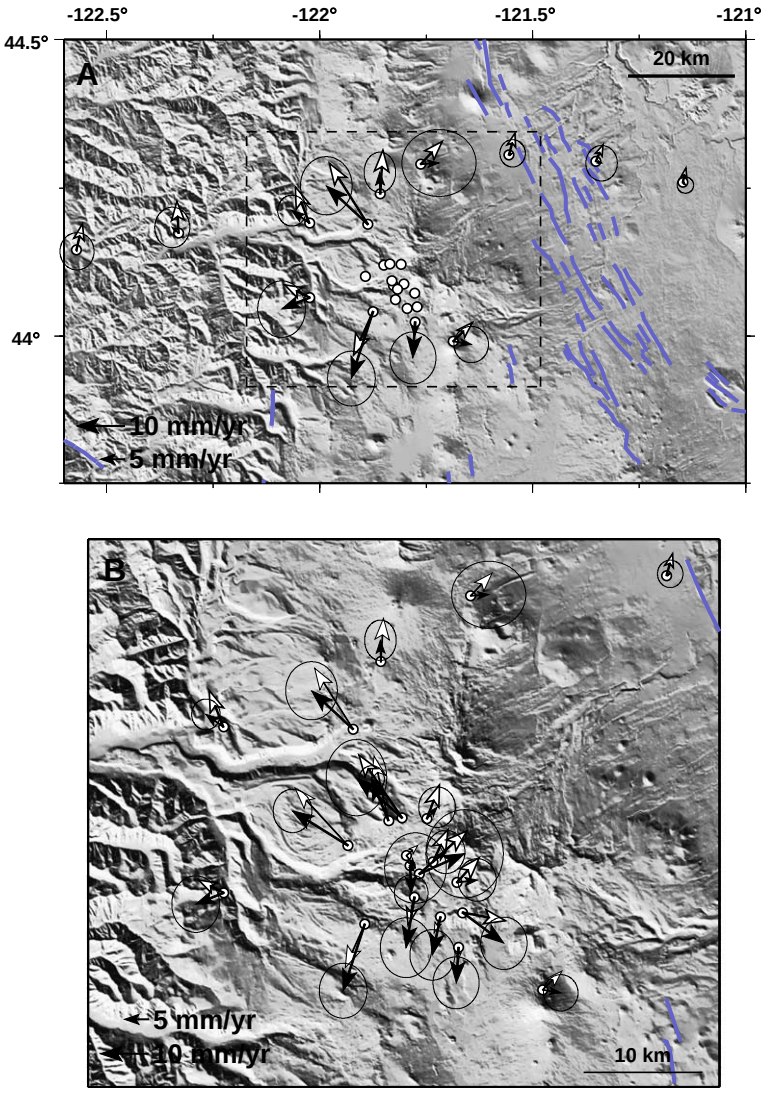

Fig. 4. Observed and corrected station velocities (white arrows and black arrows with 95% confidence ellipses, respectively) from campaign-style GPS measurements in 2001, 2002, and 2003. Dashed box in A shows the area covered in B, which includes station velocities for the central cluster of stations in A. See text and Table 3 for details.

two lines along the James Creek and Separation Creek Trails that intersect near James Creek Shelter and within 1 km of the deformation center (Fig. 1, C). To minimize the visual impact of the marks in the wilderness, we used small stainless steel pins about 10 cm long and 1.3 cm in diameter (4×0.5 in) with rounded tops for leveling and a center punch for GPS. We epoxied the pins into holes drilled into bedrock or large buried boulders to produce an average pin spacing of 385 m (ranging from 50 to 800 m). The pins project about 2 cm above the rock surface; most are not visible from the trail. The north–south line along the James Creek Trail is 7.4 km long and the east–west line along the Separation Creek Trail is 3.4 km long (stadia distances). The James Creek Shelter is about 13 km along trails from the trailhead at Devils Lake. A 3-person crew can carry the leveling equipment to or from the site in less than 1 day. Single-running both lines to first-order standards requires 3–4 days.

Table 2
Best-fit Euler vectors and uniform strains based on campaign and continuous GPS data from Svarc et al. (2002) and this study

Parameter	Svarc et al., 2002	This study
Latitude of pole, °N	43.40 ± 0.14	44.22 ± 0.15
Longitude of pole, °W	119.33 ± 0.28	118.37 ± 0.36
Angular velocity, deg Myr^{-1}	−0.822 ± 0.057	−0.818 ± 0.085
ε_{EE}, nstrain yr^{-1}	−7.4 ± 1.8	4.7 ± 1.5
ε_{EN}, nstrain yr^{-1}	−3.4 ± 1.0	−3.4 ± 1.0
ε_{NN}, nstrain yr^{-1}	−5.0 ± 0.8	−7.5 ± 1.4
Normalized variance	1.6	1.0

See text for details.

We measured the lines again in September 2003 with the results shown in Fig. 5. Relative uplift centered near James Creek Shelter is apparent in the north–south displacement profile, while the east–west profile is nearly flat. This pattern is consistent with the source location revealed by InSAR, i.e., the north–south line is centered near the deformation source and the east–west line is close to the source and too short to capture any relative vertical displacements from 2002 to 2003. For the source inversions we used relative height changes between adjacent

Table 3
Observed and corrected station velocities relative to stable North America in the Three Sisters area from campaign GPS observations in 2001, 2002, and 2003

Station	Latitude (°N)	Longitude (°E)	North velocity (mm/yr)	Corrected North velocity (mm/yr)	Standard deviation, σ_N (mm/yr)	East velocity (mm/yr)	Corrected east velocity (mm/yr)	Standard deviation σ_E (mm/yr)	Correlation between σ_N and σ_E	Vertical velocity (mm/yr)	Standard deviation σ_{UP} (mm/yr)
BKMW	44.1006	−121.8922	12.17	7.31	1.87	−11.19	−11.74	1.67	−0.06	28.22	6.76
BLCK	44.2902	−121.7630	4.77	0.26	2.89	4.51	3.87	3.20	−0.12	−9.97	9.21
BR02	44.1738	−122.3306	6.68	1.22	1.75	−0.37	−1.38	1.51	−0.04	−17.24	6.02
BRNT	44.0409	−121.8744	−9.22	−14.11	2.37	−4.13	−4.60	2.06	−0.03	13.57	8.57
C753*	44.3070	−120.6189	3.77	1.00	1.54	−0.76	−0.42	1.38	0.00	−0.59	5.10
CUPO	44.1907	−122.0238	7.64	2.65	1.33	−2.95	−3.71	1.23	−0.05	3.17	4.52
DRYX*	44.2105	−121.0858	8.86	5.31	1.28	1.41	1.45	1.14	−0.05	−3.88	4.32
HSTN*	44.2564	−120.9298	4.43	1.15	1.34	0.92	1.05	1.26	−0.07	−3.12	4.47
HUSB	44.1195	−121.8494	13.62	8.84	1.13	−3.03	−3.56	1.09	−0.02	17.81	4.09
JACR	44.0853	−121.8269	−1.03	−5.81	1.57	0.75	0.28	1.45	−0.02	30.01	5.89
KOKO	44.0463	−121.7945	−3.28	−8.04	2.18	−1.33	−1.73	1.94	−0.05	7.65	7.95
LALA	44.1891	−121.8870	12.89	8.11	2.51	−8.13	−8.77	2.23	0.14	0.63	10.58
LINT	44.2403	−121.8575	9.23	4.54	1.74	0.56	−0.10	1.36	0.05	4.25	5.48
M753*	44.3971	−120.4159	4.55	2.16	1.83	−0.25	0.17	1.51	0.00	3.98	6.00
MOSQ	44.0646	−122.0236	2.70	−2.39	2.44	−5.29	−5.91	2.06	−0.11	15.95	9.43
N735	44.2948	−121.3520	3.52	−0.37	1.53	1.52	1.24	1.36	−0.05	−5.68	5.00
PMAR	43.9907	−121.6867	4.00	−0.64	1.57	4.08	3.83	1.49	0.01	−7.76	6.32
REDM	44.2598	−121.1479	3.00	−0.61	0.70	0.64	0.57	0.71	−0.04	3.25	1.47
SINK	44.0232	−121.7757	−2.78	−7.53	2.24	−0.12	−0.48	1.99	0.02	18.59	8.44
SIST	44.3057	−121.5559	4.54	0.36	1.18	1.26	0.79	1.10	−0.03	0.85	3.92
SS01	44.0495	−121.7712	−1.75	−6.47	2.26	9.10	8.71	2.00	−0.02	2.45	8.36
SS03	44.1211	−121.8090	7.13	2.41	1.75	2.65	2.15	1.58	−0.01	18.67	6.32
SS15	44.0882	−121.8026	6.83	2.09	1.87	3.18	2.72	1.65	−0.04	11.63	6.83
SS16	44.0726	−121.7772	5.20	0.49	1.84	4.68	4.26	1.65	−0.03	1.75	6.64
TSXJ	44.0788	−121.8169	9.07	4.30	3.81	10.01	9.55	3.34	0.14	−16.18	14.64
TSXO	44.0930	−121.8305	2.13	−2.65	3.04	2.37	1.88	2.66	0.02	−1.38	12.49
TSXV	44.1215	−121.8352	13.30	8.54	3.29	−9.12	−9.64	2.61	0.09	34.23	11.94
VIDA	44.1456	−122.5706	5.55	−0.30	1.61	1.29	0.11	1.47	0.08	−4.81	5.06
WIFE	44.0613	−121.8220	−5.88	−10.67	2.58	−1.35	−1.79	2.22	−0.18	21.46	11.04

Velocities at HUSB and PMAR are from continuous observations since May 2001 and April 2002, respectively. Rigid block rotation and regional strain were removed from observed velocities to compute corrected velocities. See Fig. 1 for station locations.
* Velocities not shown in figures.

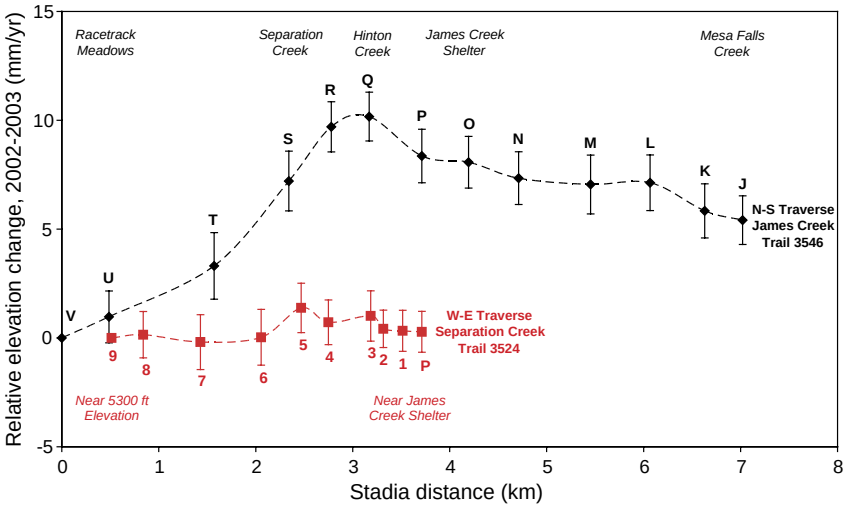

Fig. 5. Relative height changes, September 2002 to September 2003, along two short leveling lines in the Three Sisters Wilderness (Fig. 1, C). Black data points and labels (upper dataset) refer to north–south line, red data points and labels (lower dataset) refer to west–east line. Dashed lines are smoothed lines through data points, not model fits. Marks V and 9 at north and west ends, respectively, were assumed fixed to display height-change profiles shown here. However, to invert for a source model each section was treated independently (i.e., tilts between adjacent marks were used as input rather than vertical displacements relative to an assumed datum). This approach avoids covariance between height-change measurements introduced by marks that are common to adjacent sections. Stadia distance for north–south line measured from V; for west–east line, stadia distance adjusted to match value at P to north–south line. Error bars, one standard deviation from the combination of random leveling error for first-order, class II surveys and random-walk mark instability, $\sigma_\tau = (1.0\ \mathrm{mm}\cdot\mathrm{km}^{-1/2}\cdot\sqrt{L_\tau}) + (0.5\mathrm{mm}\cdot\mathrm{yr}^{-1/2}\cdot\sqrt{\Delta t})$, where L_τ is the stadia distance between adjacent marks in kilometers and Δt is the time between surveys in years. Thus, the error bars give an indication of the uncertainty in tilt τ measured between adjacent marks, which differs from the uncertainty in net height change relative to the datum point. The latter increases as $\sqrt{L}$, where L is the stadia distance from the datum point. (For interpretation of the references to colour in this figure legend, the reader is referred to the web version of this article.)

marks (i.e., mark-to-mark tilts) from both lines together with comparable data from the South Sister tilt-leveling lines (1985–1986 to 2001).

4.4. SAR interferometry, 2000–2001

The initial InSAR results were revisited and updated by Wicks et al. (2002b) and Dzurisin et al. (2003) to include interferograms for the period from October 2000 to October 2001. They selected multiple ERS-1 and ERS-2 radar images based on orbital separation and time of year to ensure good viewing geometry for interferometry and to increase the likelihood that interferometric coherence would be maintained, respectively. Experience showed that persistent snow cover destroys coherence for all but summer or early autumn scenes. A successful interferogram for the period from October 2000 to October 2001 revealed that uplift continued at an average rate of 3–4 cm/yr. Based on their analysis of all available interferograms, the authors concluded that the maximum uplift had increased to ~14 cm by October 2001, most or all of which had occurred since September 1998.

4.5. Continuous GPS, May 2001–July 2004

Responding to the discovery of uplift in April 2001 and in cooperation with the U.S. Forest Service (USFS), the USGS installed two CGPS stations: one ~2 km northwest of the deformation center near The Husband in May 2001 (HUSB) and another at Pine Marten Lodge on the north flank of Mount Bachelor, ~15 km to the southeast, in April 2002 (PMAR) (Fig. 1B). Land-use restrictions weighed against additional installations in the deforming area at that time. A swarm of about 300 small earthquakes ($M_{\max} = 1.9$) occurred in the northeast quadrant of the deforming area on March 23–26, 2004. This was the first notable seismicity in the area for at least two decades. Follow-

ing the swarm, a third CGPS station and a seismometer were permitted by the USFS and installed by the USGS near The Wife (Fig. 3) in July 2004.

4.5.1. Station velocities at PMAR and HUSB

PMAR is located near the southeast margin of the deforming area revealed by InSAR. Its velocity relative to stable North America includes the effects of clockwise block rotation in central Oregon and small seasonal variations. The seasonal signal is common to all CGPS stations in the region, so we ignored it and solved for average station velocities using linear regression. Through June 1, 2004, the mean station velocity at PMAR relative to stable North America was 4.0 ± 1.6 mm/yr north, 4.0 ± 1.5 mm/yr east, and -7.6 ± 6.3 mm/yr up (1 sigma uncertainties) (Fig. 6, right). The block rotation model of Svarc et al. (2002) for central Oregon predicts a northward velocity at PMAR of 2.7 mm/yr and an eastward velocity of 0.9 mm/yr, which agree with the observed velocities at the 2 sigma (95% confidence) level.

The HUSB data clearly show the effects of an inflation center to the southeast (i.e., motion of HUSB is generally to the northwest) plus seasonal variations similar to those seen at PMAR. The GPS antenna at HUSB was under snow from December 2003 to March 2004, which caused relatively large excursions in the time series that we excluded from the linear regression analysis. In this case, block rotation is a much smaller fraction of the total signal. The mean station velocities at HUSB are 13.6 ± 1.1 mm/yr north, -3.1 ± 1.1 mm/yr east, and 17.9 ± 4.1 mm/yr up (Fig. 6, left). We included the weighted velocities at PMAR and HUSB in our inversions (see Modeling section).

5. Modeling

We had three spatially and temporally disparate sets of data to model: (1) campaign GPS data from field surveys in 2001, 2002, and 2003; (2) leveling data from surveys in 2002 and 2003 (we did not include the tilt-leveling data from South Sister that were acquired in 1985, 1986, and 2001 because they are so few relative to the other datasets); and (3) InSAR measurements from European Space Agency ERS1 and ERS2 satellites that collectively span from 1992 to 2001. Our efforts to include post-2001 ERS2 data have been unsuccessful. We chose to model the InSAR data shown in Fig. 1. This interferogram is a stack of two ERS2 interferograms: one from Septem-

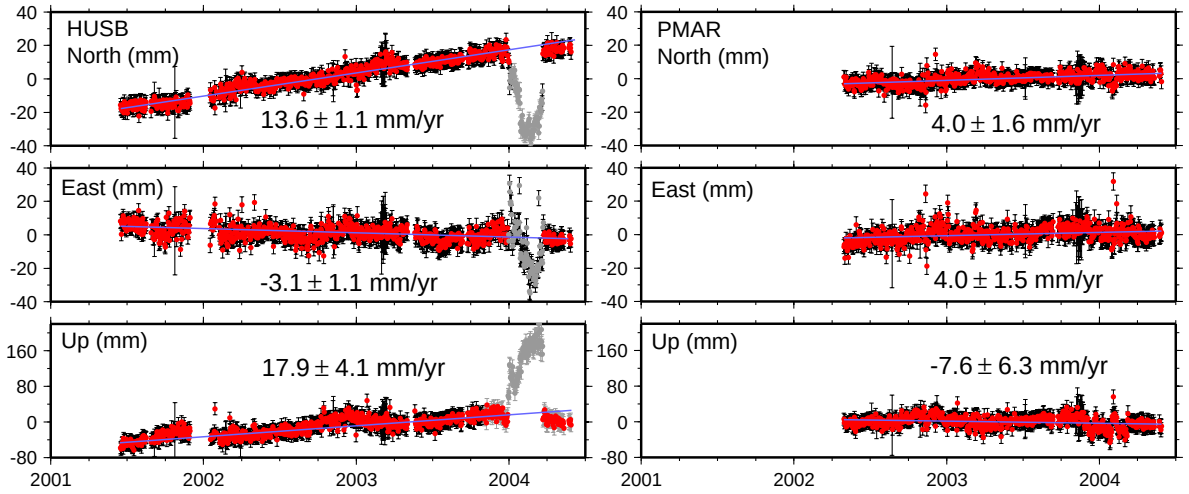

Fig. 6. North, east, and vertical components of the motion of continuous GPS stations PMAR and HUSB relative to stable North America. Error bars are one standard deviation. In late 2003 and early 2004 the GPS antenna at HUSB was covered by snow, which resulted in offsets and drift in the component time series (data shown in gray). The linear fits shown in the plots exclude these data. Other, smaller departures from linearity at both stations are recognizable as seasonal patterns that also occur in the time series from other CGPS stations in the region.

ber 1995 to October 1999, and the other from October 1999 to September 2001. To reduce the number and redundancy of the InSAR data, which otherwise would have overwhelmed the other datasets, we sub-sampled the InSAR data using the quad-tree method (Simons et al., 2002; Jónsson et al., 2002). Tilt (from orbital errors) and static shift were removed from the interferogram using data outside the deforming area (Fig. 1) before sub-sampling. Using data from outside the deforming area in this corrected interferogram, we calculated a data variance of 12 mm^2, which we used for the quad-tree cutoff. The quad-tree procedure reduces the number of InSAR data points to 672 (Fig. 7). We made the following assumptions to jointly invert the data for a best-fit deformation source:

(1) *The Earth is an isotropic homogeneous half-space*. We did not include variable topography in our joint inversion of this heterogeneous dataset. Previous inversions of InSAR data alone (Wicks et al., 2002a) found this effect to be small for the InSAR data. However, the effect could be important to accurately model the horizontal GPS data (Williams and Wadge, 2000). Heterogeneities within the crust most likely bias our model. We could estimate the variation of elastic properties with depth in the

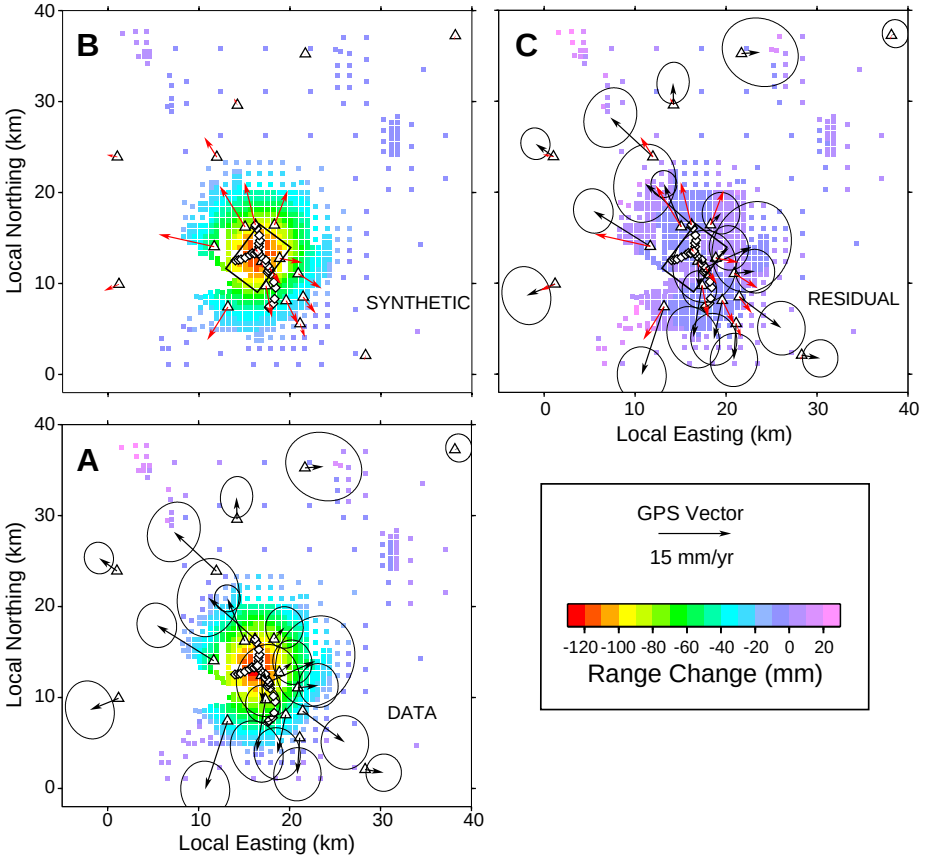

Fig. 7. GPS stations (triangles), leveling stations (diamonds) and InSAR sub-sampled points (colored squares). Black arrows in A and C represent observed GPS velocities with 95% confidence ellipses. Red arrows in B and C represent velocities calculated from the best-fit model. A, Observed GPS vectors and leveling stations plotted with the sub-sampled 1995–2001 interferogram (Fig. 1). B, Synthetic (i.e., model-derived) GPS and InSAR data with the surface projection of the best-fit model (black box). C, Residual interferogram (data minus synthetic) with observed and synthetic GPS vectors. Black box shows surface projection of best-fit model. (For interpretation of the references to colour in this figure legend, the reader is referred to the web version of this article.)

crust and approximate a layered Earth model, but considering that unknown lateral variations in this volcanic setting are likely to be as large as the vertical variations, we would only bias our models in a different direction. Clearly, a detailed tomographic model of the Three Sisters area is necessary for thorough modeling of the deformation source. Given the time scale of this uplift (ongoing since 1997 or 1998), knowledge of the underlying viscosity structure is also important for accurately modeling the deformation source.

(2) *The deformation source is simple*. The deformation signal appears to be simple (Figs. 1 and 7), which suggests a small, effectively simple source at depth. Previous modeling of the InSAR data has shown a point source model (the simplest deformation source) to be effective. In this study we modeled the combined data with a point source (Mogi, 1958), an ellipsoidal source (Yang et al., 1988; Fialko and Simons, 2000; Fialko et al., 2001), and a dislocation (dike or sill) source (Okada, 1985; Feigl and Dupré, 1999).

(3) *The location, geometry, and inflation rate of the deformation source did not change* from the time of the 1995–2001 interferogram (Fig. 1) through the time of the 2001–2003 GPS and leveling measurements. This assumption allows us to add a scaling parameter to the inversion that scales the inflation rate of the source from the field measurements (GPS+leveling) to the amount of inflation observed in InSAR measurements.

(4) To estimate confidence limits on the model parameters, we assumed that *the sub-sampled InSAR points and field data points are independent*. As result, we can rely on standard F-tests of statistical significance (e.g., Menke, 1989) to estimate 95% confidence intervals.

We used a constrained Monte Carlo approach to select a large number of different starting models (~1000 per modeling run), which were fed individually into a non-linear least-squares procedure and inverted iteratively until convergence. This approach ensured not only that we found the global minimum, but also that we found local minima that were in some cases acceptable (not significantly different from the global minimum at the 95% level). After attempting several weighting schemes, we settled on one developed by Simons et al. (2002) and Fialko (2004). First, we grouped the field data (GPS and leveling) together, then weighted the field data (M points) and sub-sampled InSAR data (N points) by applying a weighting vector with a sum of unity to each dataset:

$$\sum_{i=1}^{M,N} w_i = 1 \tag{2}$$

For the field data the individual weighting for each data point is:

$$w_i = \frac{1}{\sigma_i \sum_{j=1}^{M} \frac{1}{\sigma_j}} \tag{3}$$

where σ is the 95% confidence estimate for each measurement and M is the number of field data points: 84 total data points, including 63 GPS data points (21 stations with 3 components each) and 21 leveling data points.

For the sub-sampled InSAR data the weighting for each data point is:

$$w_i = \frac{\sqrt{n_i}}{\sum_{j=1}^{N} \sqrt{n_j}} \tag{4}$$

The weighting w_i is applied to sub-sampled point i, n_i is the number of points in the quad-tree cell from which the value for the point is derived, and n_j is the number of points in each of the N quad-tree cells.

The quantity that we are minimizing is:

$$\sum_{i=1}^{M} [\alpha w_i (o_i - c_i)]^2 + \sum_{i=1}^{N} [w_i (o_i - c_i)]^2 \tag{5}$$

M is the number of field data points and N is the number of InSAR data points (quad-tree cells). The variable o is the observed value and c is the calculated value. The weighting applied to the data in Eqs. (2)–(4) applies some degree of normalization to the datasets, but because the horizontal GPS data are important for discriminating among possible sources (Dieterich and Decker, 1975), we used the relative weighting factor α to apply heavier weighting to the

field data. To determine a value of α we inverted the data beginning with a value of 7 and decreased it in subsequent inversions until the fit to the InSAR part of the data was within the 95% level of the model that best-fit the InSAR data alone. The final value of α that fit this criterion was 1.2. The calculated values of deformation for the GPS data differed by less than 1 mm/yr compared to those calculated for $\alpha = 1.0$. The final model that best-fit the combined datasets was within the 95% level of the best-fit model for each dataset modeled alone.

In every weighting scheme we tried, a shallowly dipping dislocation source (dike or sill) fit the combined dataset better than either a point source or a

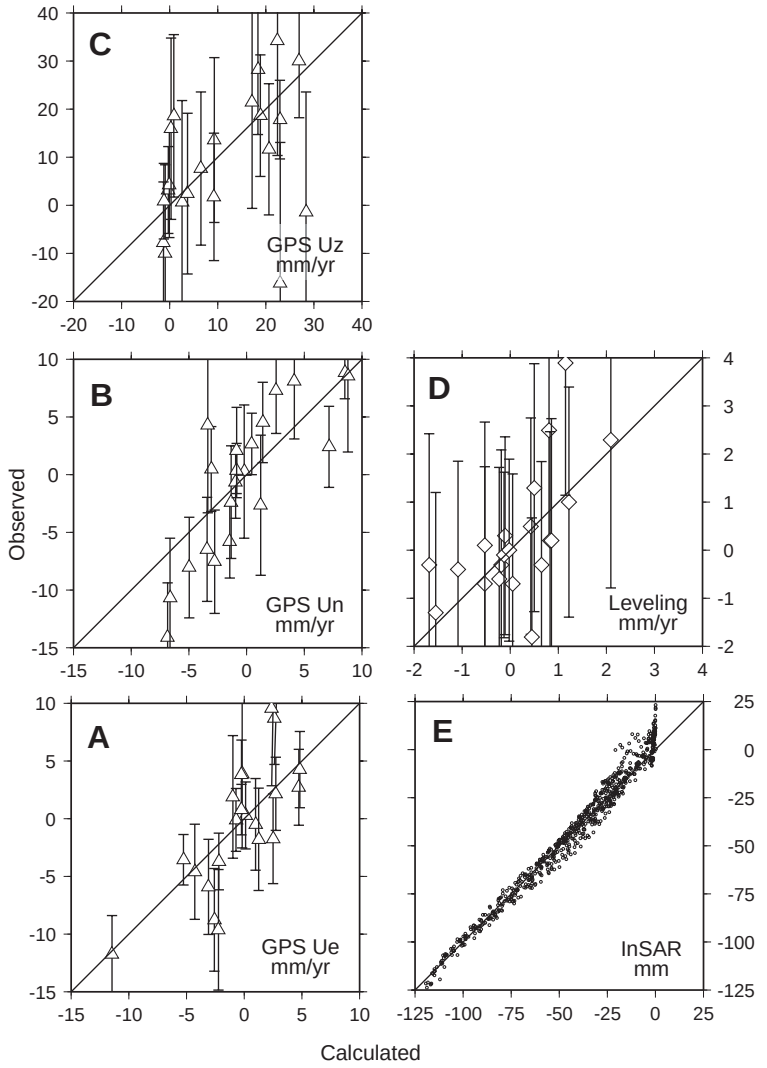

Fig. 8. Comparison of observed data (plotted on vertical axes) and synthetic data (plotted on horizontal axes) calculated for the best-fit source for three datasets. If the symbols fell on the diagonal lines, the model would perfectly explain the data. The 95% error bars are shown for the GPS and leveling data. A, Comparison of the east–west component of the GPS measurements with the synthetic data. B, Comparison of the north–south component of the GPS measurements with the synthetic data. C, Comparison of the vertical component of the GPS measurements with the synthetic data. D, Comparison of the tilt-leveling data with the synthetic data. E, Comparison of the sub-sampled InSAR data (Fig. 7, A) with the synthetic data (Fig. 7, B).

prolate ellipsoid with better than 99.99% confidence. However, because of concern that half the field data are vertical measurements that should be redundant to the InSAR data, we also performed a joint inversion using the weighting scheme described in Eqs. (2)–(5) and only the horizontal GPS and InSAR data. Again a shallowly dipping dike or sill fit the data best, with some small differences (insignificant at the 95% level) in the parameters of the source relative to the results obtained when the leveling and vertical GPS data were also included in the inversion.

Under the assumptions outlined above to determine 95% confidence limits, the best-fit model is a shallow-dipping dike or sill at a depth of 4 to 9 km, dipping 0° to 45° to the northwest. A comparison of observations and calculations is shown in Figs. 7 and 8. At the 95% level, including all acceptable models, any strike is allowed. However, the best-fit (global minimum) model has a length of ~6 km, a width of ~5 km, a depth of ~7 km, a dip of ~20 degrees to the northwest, and strikes to the northeast. Because of tradeoffs between width, length, amount of opening, and depth, it is perhaps most instructive to consider the maximum dimensions of the source and the range of volume change it represents. The maximum viable dimension of both the source length and width is ~12 km, and the range of volume added per year is from 3.5×10^6 to 6.5×10^6 m^3/yr (95% confidence limits). In our earlier study using a different set of InSAR data and a point source model (Wicks et al., 2002a,b), we estimated a yearly volume change of 6×10^6 m^3/yr. The combination of uncertainties in the depth and geometry of the source, differences among modeling approaches and weighting schemes, and assumptions about the Earth and the source make the volume-change estimate uncertain by roughly a factor of two. The scaling factor that relates the field measurements to the InSAR data ranges from 3.5 to 5.5 yr. This means the interferogram in Fig. 1 shows 3.5 to 5.5 yr of steady uplift. The CGPS station HUSB, located just north of the center of uplift (Fig. 1), shows the uplift rate to be essentially constant since the station was installed in May 2001 (Fig. 6, B). Again, assuming that the uplift has been steady since inception, the scaling factor implies that uplift began between the summer of 1996 and the summer of 1998. In an earlier study, Wicks et al. (2002a) estimated from inspection of a suite of interferograms that the uplift began between late 1997 and early 1998. The modeled total volume change during this episode through September 2003 is from 25×10^6 to 45×10^6 m^3.

European Space Agency ENVISAT data should provide InSAR measurements from 2003 on, and we may be able to fill the gap in InSAR data from 2001 to 2003 using Canadian Space Agency RADARSAT-1 data. If the inflation continues unabated and we are able to continue yearly field campaigns, we should be able to attain high quality radar data for the same time intervals. When we have datasets that are contemporaneous, we will have the confidence to attempt more rigorous modeling efforts. The misfit between the InSAR and field data (Figs. 7 and 8) may represent a violation of any (or any combination) of the assumptions listed above.

6. Discussion

Surface uplift near South Sister implies pressurization of a source, probably a shallowly dipping lens about 12 km long and 12 km wide somewhere in the depth range 4–9 km. Given the setting in an area of active volcanism, two plausible uplift mechanisms are magmatic intrusion and hydrothermal-system pressurization. Evans et al. (2004) reported a strong signature of magmatic carbon dioxide and helium in low-temperature springs along Separation Creek, which drains the uplifting area. They noted that these anomalies predate the start of uplift by at least several years, and inferred that the magmatic volatiles derive from a previous episode or multiple episodes of intrusion.

Our modeling does not rule out the alternative possibility that uplift is caused by pressurization of a preexisting hydrothermal system. However, magmatic heat input would be necessary to sustain a hydrothermal system for the two millennia that have elapsed since the last eruption at South Sister. Therefore, magmatic intrusion is required to fully explain the current uplift, whether the intrusion occurred during the past decade or at some earlier time in the geologically recent past.

Microgravity measurements are sensitive to both surface height changes and subsurface mass changes. Therefore, microgravity measurements combined with

simultaneous height-change measurements can help to distinguish between hydrothermal and magmatic uplift sources (e.g., Battaglia et al., 2003a,b). Microgravity measurements made along the leveling lines at Three Sisters in 2001 and 2002 (D.J. Johnson, unpublished data) constitute a baseline for comparison to future surveys that should help to further constrain the uplift source.

Episodic intrusions surely occur beneath the Cascade arc, as evidenced by some that erupt onto the surface. Until recently, such an intrusion probably would have escaped notice unless it produced detectable seismicity. Without InSAR, the current deformation episode would not have been recognized before the March 2004 earthquake swarm. Even then, the nature of the unrest would have remained a mystery pending the results of repeated GPS or other geodetic measurements. It follows that nearly aseismic intrusive episodes could be relatively common in the central Oregon Cascades and, until recently, have gone unnoticed.

Earthquakes are rare in central Oregon even though that segment of the Cascade arc produces more lava per kilometer than any other. The ongoing inflation episode at Three Sisters might shed some light on this apparent paradox. Wells et al. (1998) subdivided the Cascade arc into three distinct segments: 1) northern compressional (Washington), 2) central extensional (Oregon), and 3) southern transtensional (Sierra Nevada, California). The Oregon segment is characterized by low seismicity, high extrusion rate, the presence of an axial graben, and large fore-arc rotation. Relative to the Oregon segment, the Washington and Sierra Nevada segments are seismically more active with lesser fore-arc rotation and extrusion rates that are distinctly lower or somewhat lower, respectively. The axial graben in central Oregon is partly a consequence of forearc rotation, which causes extension along the trailing edge of the rotating block, i.e., along the active volcanic arc. Central Oregon is also the place where the northern margin of basin-range volcanism (the High Lava Plains) intersects the Cascade arc (Guffanti and Weaver, 1988). The resulting tectonic environment is conducive to magma intrusion, high heat flow, a shallow brittle–ductile transition (i.e., an isothermal interface between a deep hot zone where strain is accommodated mostly by aseismic creep and a shallower zone where temperatures are low enough for brittle-failure earthquakes to occur), and consequently lower seismicity than might otherwise be expected for a volcanically active area.

If the foregoing suppositions are correct, seismicity might not be a reliable indicator of intrusive activity until magma nears the surface or the intrusion rate exceeds some relatively high threshold for brittle failure. We speculate that intrusive episodes in the central Oregon Cascade Range last from days to years and are separated by quiescent periods of decades to a few centuries. Most episodes produce little or no seismicity because intrusion rates during individual episodes are not high and (or) the combination of elevated temperature (owing to frequent intrusions) and extensional setting makes the crust near the brittle–ductile transition especially accommodative to magma intrusion. In either case the high lava production rate in central Oregon results from relatively frequent intrusive episodes, mostly of small to modest size.

At present (December 2004), one of thirteen major volcanic centers in the Cascade Range is erupting (Mount St. Helens, Washington), one is known to be inflating (Three Sisters, Oregon), and two are known to be subsiding (Medicine Lake volcano and Lassen Peak, northern California). Under some circumstances, quiescent periods at Cascade volcanoes are characterized by steady subsidence, perhaps induced by cooling, volatile loss, gravitational loading, or crustal extension. For example, Medicine Lake volcano has subsided at a maximum average rate of 8.6 ± 0.9 mm/yr since the first modern leveling survey in 1954 (Dzurisin et al., 2002). Similarly, an area centered a few kilometers south of Lassen Peak subsided ~1 cm/yr from 1996 to 2000 based on InSAR results, and comparison of 1985–1986 EDM results to 2004 GPS results suggests that subsidence has persisted for two decades or more (Poland et al., 2004). Contrary to conventional wisdom, Cascade volcanoes in repose are dynamic systems that deform in response to various stimuli, including episodic intrusions that heretofore have mostly escaped detection.

Given the considerable depth of the inflation source and in the absence of additional seismicity to indicate either a significant increase in the inflation rate or the migration of magma upward into a more

brittle portion of the crust, we judge the likelihood that the current episode at Three Sisters will culminate in an eruption to be low. For reasons outlined above, magmatic intrusions are probably common beneath the Oregon Cascades but most do not reach the surface. Three possible outcomes of the current inflation episode, in order of decreasing perceived likelihood, are: (1) inflation will stop in the next several years; (2) inflation will pause and resume as a result of repeated intrusions into the same volume of the crust; and (3) the activity will persist to the point of eruption. Although an eruption in the near future is unlikely, the impact of such an event could be great. Accordingly, the USGS has completed an updated volcano hazards assessment, notified concerned agencies and the public, and is helping to prepare an emergency coordination and communication plan.

7. Conclusions

The most likely cause of surface uplift at Three Sisters in recent years is the intrusion of magma, probably basalt, into the upper crust. The depth (6.5 ± 2.5 km) and shape (shallowly dipping sill) of the best-fit source from joint inversion of InSAR, GPS, and leveling data suggest to us that intrusion is occurring along the brittle–ductile transition. The March 2004 earthquake swarm indicates that the accumulated strain is now great enough, or the strain rate was locally high enough for short time, to cause brittle failure in the epicentral zone. The intrusion rate has been roughly constant for since 1998 and there is no indication of any significant change at the time of this writing (January 2005). The ultimate outcome of this particular episode is impossible to predict, but we suspect that similar events are relatively common, though often unobserved, along the Oregon segment of the Cascade arc and that most do not culminate in eruptions.

Acknowledgements

The European Space Agency provided radar data used in this study. The authors acknowledge the considerable time and effort contributed by reviewers Willie Scott, John Langbein, Tim Melbourne, and Dan Johnson, and by guest editor Andrew Newman. Their constructive comments significantly improved the clarity of the manuscript. The USGS Volcano Hazards Program supported this research at the David A. Johnston Cascades Volcano Observatory in Vancouver, Washington, and at the USGS Western Region headquarters in Menlo Park, California.

Appendix A

The PMAR–HUSB, PMAR–WIFE, and HUSB–WIFE baselines are monitored in real-time using 3D Tracker software from Condor Earth Technologies. Carrier phase and code pseudorange observations are telemetered by radio modem from HUSB and WIFE to PMAR, and data from all three stations are retrieved via the Internet to the USGS Cascades Volcano Observatory in Vancouver, Washington. There, a delayed-state Kalman filter running on a PC processes the phase data as triple differences and the code data as double differences to obtain 10-s epoch-by-epoch solutions (Remondi and Brown, 2000; Rutledge and others, 2001). This strategy is free of errors introduced by satellite clocks, receiver clocks, atmospheric propagation delays, and initial cycle ambiguities, which makes it robust in terms of surviving cycle slips and well-suited to volcano monitoring. It does not converge on a subcentimeter position as quickly as alternative strategies that rely on double-differences, but it provides nearly instantaneous motion detection once the solution does converge. An important advantage in this situation is the software's capability to detect significant strain-rate changes automatically and in near-real time, and to notify the user by email or pager.

Note added in proof

Leveling and GPS surveys in September 2004 showed that surface deformation continued at essentially the same location and rate as in previous years. No additional earthquake swarms occurred through December 2004, while previously established trends in the CGPS data from stations HUSB and WIFE continued.

References

Balazs, E.I., Young, G.M., 1982. Corrections applied by the National Geodetic Survey to precise leveling observations. NOAA Tech. Memo. 34 (12 pp.).

Battaglia, M., Segall, P., Murray, J., Cervelli, P., Langbein, J., 2003a. The mechanics of unrest at Long Valley caldera, California: 1. Modeling the geometry of the source using GPS, leveling and 2-color EDM data. J. Volcanol. Geotherm. Res. 127, 195–217.

Battaglia, M., Segall, P., Roberts, C., 2003b. The mechanics of unrest at Long Valley caldera, California: 2. Constraining the nature of the source using geodetic and micro-gravity data. J. Volcanol. Geotherm. Res. 127, 219–245.

Berg Jr., J.W., Baker, C.D., 1963. Oregon earthquakes, 1941 through 1958. Bull. Seismol. Soc. Am. 53, 95–108.

Dieterich, J.H., Decker, R.W., 1975. Finite element modeling of surface deformation associated with volcanism. J. Geophys. Res. 80, 4094–4102.

Dong, D., Herring, T.A., King, R.W., 1998. Estimating regional deformation from a combination of space and terrestrial geodetic data. J. Geodesyn. 72, 200–214.

Dzurisin, D., Poland, M.P., Burgmann, R., 2002. Steady subsidence of Medicine Lake volcano, northern California, revealed by repeated leveling surveys. J. Geophys. Res. 107 (B12), 2372. doi:10.1029/2001JB000893.

Dzurisin, D., Endo, E., Iwatsubo, E., Lisowski, M., Poland, M., Wicks Jr., C., 2003. New results from a proposed PBO Cascade volcano cluster II: InSAR, GPS, and tilt-leveling data from the Three Sisters area, central Oregon [abstract]. 2003 Seattle Annual Meeting (November 2–5, 2003), Seattle, Washington, p. 563.

Evans, W.C., van Soest, M.C., Mariner, R.H., Hurwitz, S., Ingebritsen, S.E., Wicks Jr., C.W., Schmidt, M.E., 2004. Magmatic intrusion west of Three Sisters, central Oregon, USA: the perspective from spring chemistry. Geology 32, 69–72.

Federal Geodetic Control Committee, 1984. Bossler, J.D. (chairman), Standards and specifications for geodetic control networks. National Oceanic and Atmospheric Administration, Rockville, Maryland.

Feigl, K., Dupré, E., 1999. RNGCHN: a program to calculate displacement components from dislocations in an elastic half-space with applications for modeling geodetic measurements of crustal deformation. Comput. Geosci. 25, 695–704.

Fialko, Y., 2004. Probing the mechanical properties of seismically active crust with space geodesy: Study of the co-seismic deformation due to the 1992 M_w7.3 Landers (southern California) earthquake. J. Geophys. Res. 109. doi:10.1029/2003JB002756.

Fialko, Y., Simons, M., 2000. Deformation and seismicity in the Coso geothermal area, Inyo County, California: observations and modeling using satellite radar interferometry. J. Geophys. Res. 105, 21,781–21,794.

Fialko, Y., Simons, M., Khazan, Y., 2001. Finite source modeling of magmatic unrest in Socorro, New Mexico, and Long Valley, California. Geophys. J. Int. 146, 191–200.

Fierstein, J., Calvert, A., Hildreth, W., 2003. Two young silicic sisters at Three Sisters volcanic field, Oregon. Abstr. Programs-Geol. Soc. Am. 35 (6), 563 September 2003.

Guffanti, M., Weaver, C.S., 1988. Distribution of Late Cenozoic volcanic vents in the Cascade Range: volcanic arc segmentation and regional tectonic considerations. J. Geophys. Res. 93 (B6), 6513–6529.

Ingebritsen, S.E., Mariner, R.H., Sherrod, D.R., 1994. Hydrothermal systems of the Cascade Range, north-central Oregon. U.S. Geol. Surv. Prof. Pap. 1044-L (86 pp.).

Iverson, J.T., 1999, An investigation of the chloride anomaly in Separation Creek, Lane County, Oregon, B.S. thesis, Oregon State University, Corvallis, OR.

Iwatsubo, E.Y., Topinka, L., Swanson, D.A., 1988. Measurements of slope distances and zenith angles at Newberry and South Sister volcanoes, Oregon, 1985–1986. Geol. Surv. Open-File Rep. 88-377 (51 pp.).

Jónsson, S., Zebker, H., Segall, P., Amelung, F., 2002. Fault slip distribution of the 1999 M_w 7.1 Hector Mine, California, earthquake, estimated from satellite radar and GPS measurements. Bull. Seismol. Soc. Am. 92, 1377–1389.

Lisowski, M., Prescott, W.H., 1981. Short-range distance measurements along the San Andreas fault system in California, 1975–1979. Bull. Seismol. Soc. Am. 71 (5), 1607–1624.

McCaffrey, R.M., Long, M.D., Goldfinger, C., Zwick, P.C., Nableck, J.L., Johnson, C.K., Smith, C., 2000. Rotation and plate locking at the southern Cascadia subduction zone. Geophys. Res. Lett. 27, 3117–3120.

Menke, W., 1989, Geophysical data analysis: discrete inverse theory, 289 p., Academic Press Inc., Harcourt Brace Jovanovich Publishers, San Diego.

Mogi, K., 1958. Relations between the eruptions of various volcanoes and the deformation of the ground surfaces around them. Bull. Earthq. Res. Inst. Univ. Tokyo 36, 99–134.

Muffler, L.J.P., Nehring, N.L., Truesdell, A.H., Janik, C.J., Clynne, M.A., Thompson, J.M., 1982. The Lassen geothermal system. Proceedings of the Pacific Geothermal Conference, Auckland, New Zealand, 8–12 Nov., pp. 349–356.

Okada, Y., 1985. Surface deformation due to shear and tensile faults in a half-space. Bull. Seismol. Soc. Am. 75, 1135–1154.

Poland, M., Bawden, G., Lisowski, M., Dzurisin, D., 2004. Newly discovered subsidence at Lassen Peak, southern Cascade Range, California, from InSAR and GPS. EOS Trans. AGU 85 (47) (Fall Meet. Suppl. Abstract G51A-00680).

Remondi, B.W., Brown, G., 2000. Triple differencing with Kalman filtering: making it work. GPS Solut. 3 (3), 58–64.

Rutledge, D., Gnipp, J., Kramer, J., 2001. Advances in real-time GPS deformation monitoring for landslides, volcanoes, and structures. Proceedings of the 10th FIG International Symposium on Deformation Measurementsm, Orange, California, March 19–22, pp. 110–121.

Savage, J.C., Lisowski, M., Prescott, W.H., 1996. Observed discrepancy between geodolite and GPS distance measurements. J. Geophys. Res. 101 (B11), 25,547–25,552.

Savage, J.C., Gan, W., Svarc, J.L., 2001a. Strain accumulation in the Eastern California Shear Zone. J. Geophys. Res. 106 (B10), 21,995–22,007.

Savage, J.C., Svarc, J.L., Prescott, W.H., 2001b. Strain accumulation near Yucca Mountain, Nevada, 1993–1998. J. Geophys. Res. 106, 16,483–16,488.

Scott, W.E., Gardner, C.A., 1990. Field trip guide to the central Oregon High Cascades: part 1, Mount Bachelor-South Sister area. Or. Geol. 52 (5), 99–114.

Scott, W.E., Iverson, R.M., Schilling, S.P., Fischer, B.J., 2001. Volcano hazards in the Three Sisters region, Oregon. U.S. Geol. Surv. Open-File Rep. 99-437 (14 pp.).

Sherrod, D.R., Smith, I.G., 1990. Quaternary extrusion rates of the Cascade Range, northwestern United States and southern British Columbia. J. Geophys. Res. 95, 19,465–19,474.

Simons, M., Fialko, Y., Rivera, L., 2002. Coseismic deformation from the 1999 M_w 7.1 Hector Mine, California, earthquake, as inferred from InSAR and GPS observations. Bull. Seismol. Soc. Am. 92, 1390–1402.

Svarc, J.L., Savage, J.C., Prescott, W.H., Murray, M.H., 2002. Strain accumulation and rotation in western Oregon and southwestern Washington. J. Geophys. Res. 107. doi:10.1029/2001/JB000625.

Taylor, E.M. MacLeod, N.S. Sherrod, D.R. Walker, G.W., 1987. Geologic map of the Three Sisters Wilderness, Deschutes, Lane, and Linn counties, Oregon. U.S. Geol. Surv. Misc. Field Studies Map, MF-1952.

Weaver, C.S., Michaelson, C.A., 1985. Seismicity and volcanism in the Pacific Northwest: evidence for the segmentation of the Juan de Fuca plate. Geophys. Res. Lett. 12, 215–218.

Wells, R.E., Weaver, C.S., Blakely, R.J., 1998. Fore arc migration in Cascadia and its neotectonic significance. Geology 26, 759–762.

Wicks Jr., C.W., Dzurisin, D., Ingebritsen, S., Thatcher, W., Lu, Z., Iverson, J., 2002a. Magmatic activity beneath the quiescent Three Sisters volcanic center, central Oregon Cascade Range, USA. Geophys. Res. Lett. 29 (7), 26-1–26-4.

Wicks, C.W., Dzurisin, D., Ingebritsen, S., Thatcher, W., Lu, Z., Iverson, J., 2002b. Ongoing magma intrusion beneath the Three Sisters volcanic center, central Oregon Cascade Range, USA, inferred from satellite InSAR [abstract]. Geological Society of America, Cordilleran Section, 98th annual meeting, May 13–15, 2002, Abstracts with Programs, vol. 34 (5), pp. 90–91.

Williams, C.A., Wadge, G., 2000. An accurate and efficient method for including the effects of topography in three-dimensional elastic models of ground deformation with applications to radar interferometry. J. Geophys. Res. 105, 8103–8120.

Yamashita, K.M., Doukas, M.P., 1987. Precise level lines at Crater Lake, Newberry Crater, and South Sister, Oregon. U.S. Geol. Surv. Open-File Rep. 87-293 (32 pp.).

Yang, X.-M., Davis, P., Dietrich, M., 1988. Deformation from inflation of a dipping finite prolate spheroid in an elastic half-space as a model for volcanic stressing. J. Geophys. Res. 93, 4249–4257.

Zumberge, J.F, Heflin, M.B., Jefferson, D.C., Watkins, M.M., Webb, F.H., 1997. Precise point positioning for the efficient and robust analysis of GPS data from large networks. J. Geophys. Res. 102 (B3), 5005–5017.